CONFERENCE PRE-PRINT

CHARACTERISTICS OF RUNAWAY ELECTRON LOSS IN THE INTEGRATED COMMISSIONING OF JT-60SA

S. SUMIDA
Naka Institute for Fusion Science and Technology, National Institutes for Quantum Science and Technology
Ibaraki, Japan
Email: sumida.shuhei@qst.go.jp

K. SHINOHARA
Department of Complexity Science and Engineering, The University of Tokyo
Chiba, Japan
Naka Institute for Fusion Science and Technology, National Institutes for Quantum Science and Technology
Ibaraki, Japan

A. M. SUKEGAWA
Naka Institute for Fusion Science and Technology, National Institutes for Quantum Science and Technology
Ibaraki, Japan

T. NISHITANI
Graduate School of Engineering, Nagoya University
Nagoya, Japan

K. OGAWA, M. ISOBE
National Institute for Fusion Science, National Institutes of Natural Sciences
Gifu, Japan
Department of Fusion Science, The Graduate University for Advanced Studies, SOKENDAI
Gifu, Japan

S. KONO, M. ISHIKAWA, H. HOMMA, M. SUEOKA, T. YOKOYAMA, S. KOJIMA,
S. INOUE, M. TAKECHI, K. KAMIYA, K. KOBAYASHI and M. YOSHIDA
Naka Institute for Fusion Science and Technology, National Institutes for Quantum Science and Technology
Ibaraki, Japan

Abstract

Spatiotemporal characteristics of runaway electron (RE) loss on plasma facing components (PFCs) have been investigated with neutron flux monitors in the integrated commissioning of the largest superconducting tokamak JT-60SA, where the available toroidal electric field is limited to be low as well as that in ITER and DEMO. Even in the low toroidal electric field tokamak, REs are found to be generated and lost in the case when plasma density is low, when plasma hit the wall or when intense MHD modes are present. In addition, spatial locality of the RE loss on the PFC is confirmed based on a magnitude relation of neutron flux monitor's signals.

1. INTRODUCTION

Runaway electrons (REs) are high-energy electrons generated by a strong toroidal electric field in low-density plasma, for instance, at tokamak plasma startup or disruption. When REs are lost locally on the plasma facing components (PFCs), intense heat loads are caused there. This is one of the crucial issues in terms of machine protection for future tokamaks such as ITER and DEMO [1]. Before safe plasma operation scenarios are experimentally established, REs would be generated and lost on PFCs. The available toroidal electric field is limited to be low in large superconducting tokamaks. JT-60SA is the currently largest superconducting tokamak in the world and comparable in scale to ITER and DEMO. The first plasma campaign in JT-60SA called the integrated commissioning was conducted in 2023 [2]. In the case of the integrated commissioning of JT-60SA, the available toroidal electric field is 0.15 V/m, which is lower than that in ITER [3]. It is important to understand how REs are generated and lost in the first plasma campaign of such a low toroidal electric field machine in order to consider avoidance or mitigation methods of the local RE losses in the first campaign of ITER and DEMO. The objective of this study is to characterize RE losses in the integrated commissioning of JT-60SA.

2. DETECTION METHOD OF RE LOSS

When REs collide with PFCs, gamma rays are generated as bremsstrahlung. The gamma-rays produce photoneutrons via nuclear reaction with atoms in in-vessel components [4]. Although gamma-ray diagnostics are useful to measure RE losses, there was no dedicated gamma-ray diagnostics installed in JT-60SA at the integrated commissioning phase. In the integrated commissioning of JT-60SA, no fusion neutron is produced in the plasma because bulk ion species of the plasma are only H or He. The RE loss can be detected through measurement of the photoneutrons instead of the gamma rays. Thus, in this study, we utilized neutron flux monitors (NFMs) to indirectly detect RE losses on PFCs via measurement of the photoneutrons. Since the available spaces for plasma diagnostics are limited, installation of dedicated RE diagnostics is optional, or low priority in the current design of JA-DEMO. On the other hand, NFM will be installed for measurement of fusion neutrons in JA-DEMO. If NFM is demonstrated to work as RE diagnostics in the integrated commissioning of JT-60SA, NFM can be treated as an attractive candidate for RE diagnostics in the non-activation phase of JA-DEMO.

The NFMs are installed at P-10 and P-18 horizontal ports (160 degrees apart at a toroidal angle) in the integrated commissioning of JT-60SA. Figure 1 shows a schematic drawing of a NFM in JT-60SA. Structures of NFMs at P-10 (NFM10) and P-18 (NFM18) are identical. The detector of the NFM is a ^{235}U fission chamber. The fission chamber is KSA type of TOSHIBA Electron Tubes and Devices Co., LTD, which is also used as a detector of NFM in JT-60U [5] and LHD [6]. A 50-mm-thick polyethylene moderator is placed around the detector to detect fast neutrons. To avoid the detection efficiency of thermal neutrons, a 1-mm-thick Cd shield is placed.

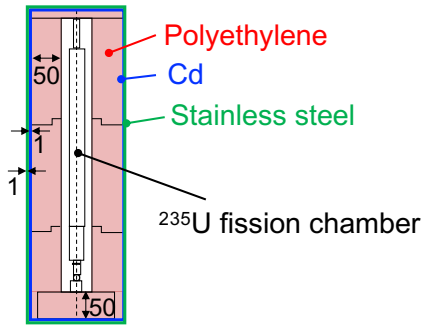

FIG. 1. Schematic drawing of a neutron flux monitor (NFM) in JT-60SA. The NFM consists of a ^{235}U fission chamber, a 5-mm-thick polyethylene moderator, a 1-mm-thick Cd shield and a 1-mm-thick stainless-steel housing.

3. CHARACTERISTICS OF OBSERVED RE LOSS

In the integrated commissioning of JT-60SA, RE losses are observed both when MHD activity with toroidal mode number n = 1, which is considered as a tearing mode [7], is present and when it is absent. When the n = 1 MHD mode is present, there is a temporal correlation between the RE loss and the n = 1 mode. Characteristics of the observed RE loss in each case are described below.

3.1. RE loss without n = 1 MHD mode

First, we show a typical discharge where RE losses are observed under the case without the n = 1 mode. Its time evolution is shown in Fig. 2. In this time period, there is no intense n = 1 mode. The plasma current I_p and the toroidal loop voltage V_{loop} are almost constant. Here, the plasma density measured with the tangential CO_2 laser interferometer [8] increases gradually due to gas puffing. Neutron counting rates indicating RE losses are detected continuously in this phase. The toroidal electric field in the plasma E_{tor} is given by,

$$E_{tor} = \frac{V_{loop} - L_p dI_p/dt}{2\pi R_0}, \quad (1)$$

where L_p is the plasma inductance and R_0 is the major radius of the plasma. Here, L_p is given by $L_p = \mu_0 R_0 \left(\ln\frac{8R_0}{a} + \frac{l_i}{2} - 2\right)$, where μ_0 is the vacuum permeability, a is the plasma minor radius and l_i is the internal inductance per unit length. This l_i is evaluated based on the measurement results of the diamagnetic loops [9]. In the stationary phase of I_p, dI_p/dt is almost 0. Thus, we evaluate E_{tor} as $E_{tor} = V_{loop}/2\pi R_0$ here. Although E_{tor} is only ~0.05 V/m, the RE loss rate increases. On the other hand, the plasma density is lower than

10^{19} m^{-3} even at t = 5.7 s because an optical length of the density measurement in the plasma L is around 14 m [8]. In general, REs are generated by the Dreicer process and/or the avalanche one when the plasma density is low and the toroidal electric field is finite. These processes may cause the increase of the RE loss signal.

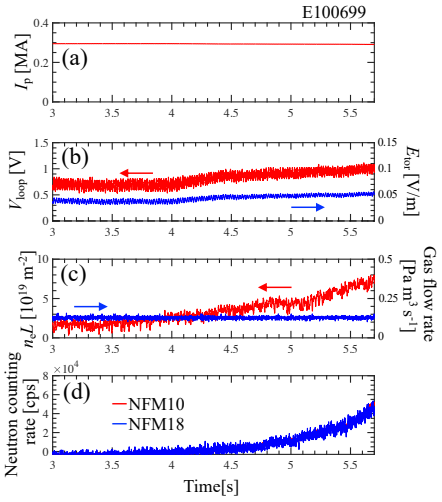

FIG. 2. Time evolution of (a) the plasma current I_p, (b) toroidal loop voltage V_{loop} (red) and toroidal electric field E_{tor} (blue), (c) line-integrated density n_eL (red) and gas flow rate (blue) and (d) neutron counting rates measured with NFM10 (red) and NFM18 (blue) in a typical discharge where RE losses are observed (E100699).

Next, we discuss the RE generation mechanism. Here, plasma parameters including the toroidal electric field are assumed to be uniform in the plasma. Figure 3(a) shows the time evolution of the Connor-Hastie critical electric field E_R and the Dreicer electric field E_D in the same discharge as that in Fig. 2. These critical and Dreicer electric fields are evaluated by $E_R = \frac{\overline{n_e} e^3 \ln\Lambda}{4\pi\varepsilon_0^2 m_e c^2}$ and $E_D = \frac{\overline{n_e} e^3 \ln\Lambda}{4\pi\varepsilon_0^2 T_e}$, where $\overline{n_e}$ is the line-averaged density at L = 14 m, e is the elementary electric charge, $\ln\Lambda$ is the Coulomb logarithm, ε_0 is the permittivity of vacuum, m_e is the electron mass, c is the speed of light and T_e is the effective electron temperature. The effective temperature is measured along the line of sight through the plasma center by the soft x-ray diagnostics [10]. Here, we assume $\ln\Lambda$ = 16. The ratios of E_{tor} to E_R and E_D are higher than 11 and 0.014, respectively. Figure 3(b) shows the evaluated RE generation rate in the Dreicer process. The Dreicer generation rate dn_{RE}/dt can be evaluated by [11],

$$\frac{dn_{RE}}{dt} = \frac{\overline{n_e}}{\tau}\left(\frac{m_e c^2}{2T_e}\right)^{3/2}\left(\frac{E_D}{E_{tor}}\right)^{3(1+Z_{eff})/16}\exp\left(-\frac{E_D}{4E_{tor}} - \sqrt{\frac{(1+Z_{eff})E_D}{E_{tor}}}\right), \quad (2)$$

where, $\tau = 4\pi\varepsilon_0^2 m_e^2 c^3/\overline{n_e} e^4 \ln\Lambda$ and Z_{eff} is the effective electric charge. Here, cases of Z_{eff} = 2, 3 and 4 are calculated. Note that the vertical axis of Fig. 3(b) is logarithm. The Dreicer generation rate drastically decreases while the RE loss rates keep increasing exponentially as shown in Fig. 3(d). This result indicates that the increase of the RE loss cannot be explained by the Dreicer process. Solid curves in Fig. 3(c) shows the evaluated RE growth rate in the avalanche process. The avalanche growth rate $\frac{1}{n_{RE}}\frac{dn_{RE}}{dt}$ can be evaluated by [12],

$$\frac{1}{n_{RE}}\frac{dn_{RE}}{dt} = \frac{1}{\tau\ln\Lambda}\sqrt{\frac{\pi}{3(5+Z_{eff})}}\left(\frac{E_{tor}}{E_R} - 1\right)\left(1 - \frac{E_R}{E_{tor}} + \frac{4\pi(Z_{eff}+1)^2}{3(Z_{eff}+5)(E_{tor}^2/E_R^2+3)}\right)^{-1/2}, \quad (3)$$

The increase rate of the RE loss rate is also shown in Fig. 3(c) as the dashed line. This increase rate is evaluated by fitting the neutron counting rates in Fig. 3(d) with an exponential function during t = 5-5.7 s. The fitted function of NFM10's signal is almost identical to that of NFM18's one. There are only about 3 times difference between the avalanche growth rate and the increase rate of RE loss, indicating they are roughly consistent. It is found that the cause for the increase of the observed RE loss rate is increase in the number of REs by the avalanche process.

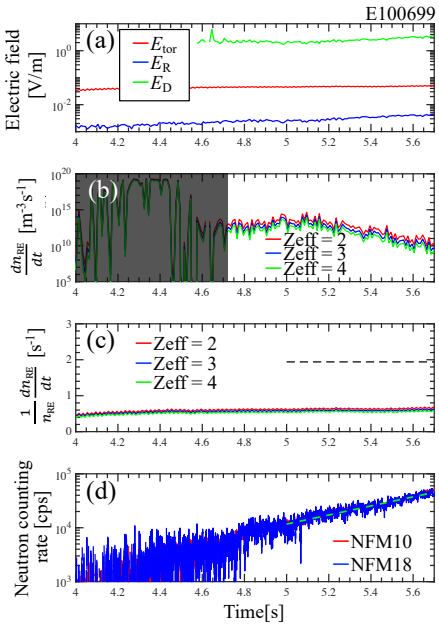

FIG. 3. Time evolution of (a) E_{tor} (red), the critical electric field E_R (blue) and the Dreicer electric field E_D (green), (b) Dreicer generation rate dn_{RE}/dt, (c) avalanche growth rate $1/n_{RE}\times dn_{RE}/dt$, and (d) neutron counting rates measured with NFM10 (red) and NFM18 (blue) in the typical discharge where the RE losses are observed (E100699). In panels (b) and (c), red, blue and green lines represent cases of Z_{eff} = 2, 3 and 4, respectively. Since measurement errors of the effective temperature are significantly large until t ~ 4.7 s, the Dreicer generation rate in the shaded area in (b) is not discussed here. The dashed line in (c) indicates the increase rate of the RE loss evaluated by fitting the neutron counting rates with an exponential function during t = 5-5.7 s.

Bursty RE losses are observed at the plasma termination phase under the condition where the $n = 1$ mode is absent. Figure 4 shows its typical discharge. This plasma is terminated by vertical displacement event (VDE). The plasma goes upward and hits the PFC. From here, E_{tor} is evaluated by $E_{\mathrm{tor}} = \frac{V_{\mathrm{loop}} - L_{\mathrm{p}} dI_{\mathrm{p}}/dt}{2\pi R_0}$ because dI_{p}/dt is finite at the analyzed time period. E_{tor} begins increasing from $t \sim 11.60$ s. At almost the same time, the bursty RE losses also begin to be detected. This bursty RE loss is considered to be caused by this increase of E_{tor}. The high E_{tor} would be due to an increase in plasma resistivity caused by the plasma hitting the PFC since particles from the PFC can cool the plasma.

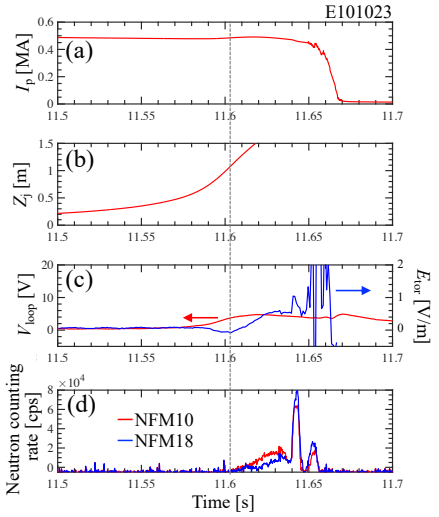

FIG. 4. Time evolution of (a) I_p, (b) vertical position of the plasma current centroid Z_j, (c) V_{loop} (red) and E_{tor} (blue) and (d) neutron counting rates measured with NFM10 (red) and NFM18 (blue) in a typical discharge where bursty RE losses are observed (E101023).

3.2. RE losses with $n = 1$ MHD mode

RE losses and the $n = 1$ MHD activity are simultaneously observed. Figure 5 shows its typical discharge. In this time period until $t \sim 5.65$ s, the plasma current decreases with several current spikes. The plasma position is almost stationary. After $t \sim 5.65$ s, VDE occurs, and the plasma moves upward. At the timing of the current spikes before $t \sim 5.65$ s, E_{tor} fluctuates due to large dI_p/dt. In the early phase of this time period ($t < 5.41$ s), the RE loss is continuously detected. (see Fig. 7(d)). In the later phase ($t > 5.41$ s) and until the VDE ($t < 5.65$ s), the RE loss signal is bursty.

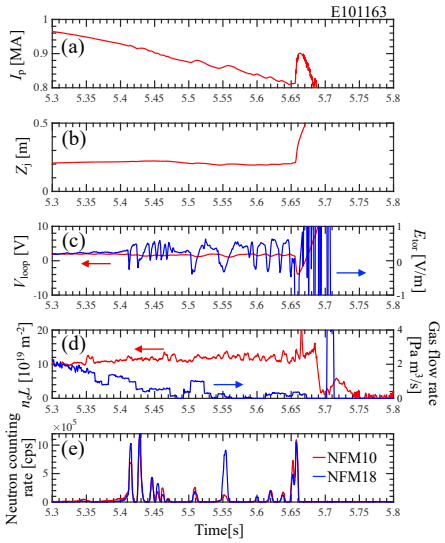

FIG. 5. Time evolution of (a) I_p, (b) Z_j, (c) V_{loop} (red) and E_{tor} (blue), (d) n_eL (red) and gas flow rate (blue) and (e) neutron counting rates measured with NFM10 (red) and NFM18 (blue) in a typical discharge where RE losses and the n = 1 mode are simultaneously observed (E101163).

Figure 6 shows the MHD activities measured by a magnetic probe [13] in the same discharge as that in Fig. 5. The MHD modes are continuously observed until $t \sim 5.41$ s and become bursty after $t \sim 5.41$ s. The mode with a toroidal mode number $n = 1$ is dominant. This mode is considered to be a tearing mode based on a radial tearing parity structure which is observed with the soft-x ray array diagnostics [7].

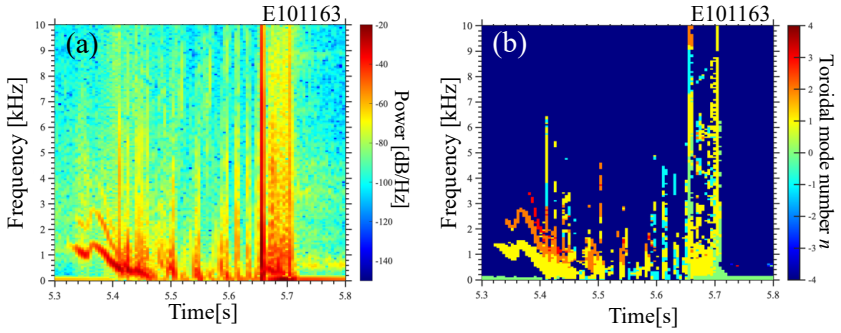

FIG. 6. Time evolution of (a) the power density spectrum and (b) their toroidal mode numbers n in E101163.

First, we discuss the relation between the continuously observed RE loss and the $n = 1$ mode. Figure 7 shows the time evolution of the discharge only in the early phase of the time period shown in Figs. 5 and 6. During $t = 5.3$-5.41 s, E_{tor} and the plasma density are almost constant, indicating that the RE generation source is also almost constant in terms of the Dreicer and avalanche processes. On the other hand, the $n = 1$ mode amplitude and the RE loss rates vary at the same time, i.e., the RE loss rate correlates with the $n = 1$ mode amplitude. It is found that the RE loss is enhanced by radial transport of REs by the $n = 1$ mode. This is because the RE loss rate cannot be increased without radial transport when the RE source is constant.

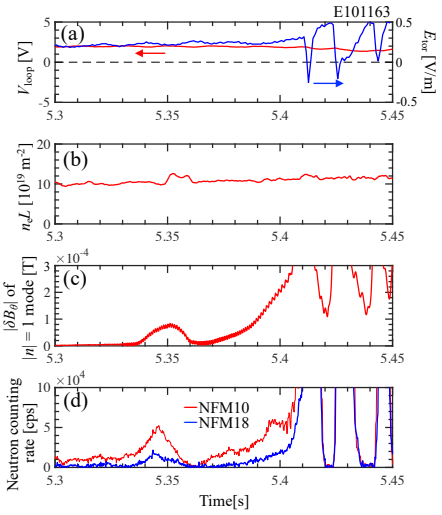

FIG. 7. Time evolution of (a) V_{loop} (red) and E_{tor} (blue), (b) n_eL, (c) magnetic fluctuation amplitude $|\delta B_\theta|$ of $|n|$ = 1 mode and (d) neutron counting rates measured with NFM10 (red) and NFM18 (blue) at t = 5.3-5.45s in the discharge where the RE losses and the n = 1 mode are simultaneously observed continuously (E101163).

Next, we discuss the relation between the bursty RE loss and the n = 1 mode. Figure 8 shows the time evolution of the discharge only in the later phase of the time period shown in Figs. 5 and 6. The plasma density is almost constant, while E_{tor} varies significantly, indicating change in the RE source in terms of the Dreicer and avalanche processes.

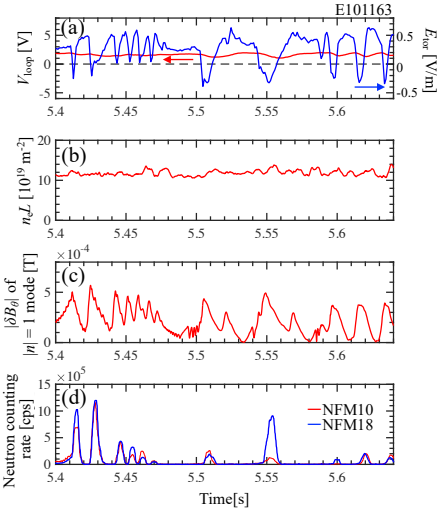

FIG. 8. Time evolution of (a) V_{loop} (red) and E_{tor} (blue), (b) n_eL, (c) $|\delta B_\theta|$ of $|n|$ = 1 mode and (d) neutron counting rates measured with NFM10 (red) and NFM18 (blue) at t = 5.4-5.64s in the discharge where the bursty RE losses and the n = 1 mode are simultaneously observed (E101163).

We compare peak values between the n = 1 mode amplitude shown in Fig. 8(c) and the bursty RE loss rate in Fig. 8(d). Figure 9 shows that the comparison result. It is found that there is a positive correlation. Therefore, the bursty RE losses are caused by the RE generation and/or the radial transport by the n = 1 mode. Influences of the MHD modes on the RE losses similar to those in this study have been also observed in other devices [14]. It is found that even in the low toroidal electric field machine, REs are generated and lost in the case of the low-density plasma, the plasma hitting PFC and the existence of the intense MHD mode.

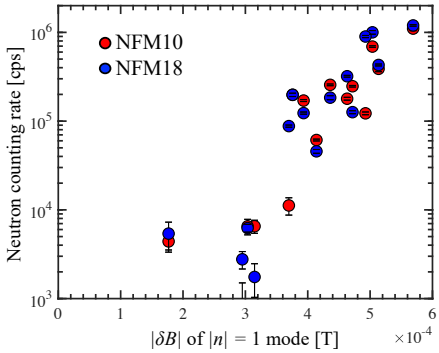

FIG. 9. Relation between magnetic fluctuation amplitude $|\delta B_\theta|$ of $|n|$ = 1 mode and neutron counting rates. Red and blue circles represent the cases where the neutron counting rates are measured with NFM10 and NFM18, respectively.

4. LOCALITY OF RE LOSS

Here, we discuss spatial characteristics of the RE loss. It can be expected that NFM's signal increases when the photoneutron generation position, namely the RE loss location, becomes closer to the NFM. If spatial distribution of the RE loss is non-uniform, a magnitude relation of the neutron counting rates between two NFMs can vary. A vertical position of NFM10, Z_{NFM10} and that of NFM18, Z_{NFM18} are around -1.0 m and -0.47 m, respectively. If REs are lost locally, the magnitude relation of NFM's signals may depend on the vertical position of the RE loss. Figure 10 shows a typical discharge where the plasma moves vertically due to VDE and the REs are lost continuously. Note that a toroidal mode number of the VDE is 0, i.e., the plasma displacement is uniform in the toroidal direction. In this time period, a magnitude relation between NFM10 and NFM18, NFM18/NFM10 fluctuates in the same way as the vertical movement of the plasma. Since $Z_{\mathrm{NFM18}} > Z_{\mathrm{NFM10}}$, change in the magnitude relation may reflect to that in the vertical RE loss position on PFC. From $t \sim 7.25$ s, a neutron counting rate of NFM18 begins decreasing while that of NFM10 continues increasing. At this timing, the vertical position of the RE loss $Z_{\mathrm{RE\ loss}}$ may deviate from Z_{NFM18} downward. There is a possibility that $Z_{\mathrm{RE\ loss}}$ is equal to Z_{NFM18} at $t \sim 7.25$ s. Thus, we assume $Z_{\mathrm{RE\ loss}} \equiv Z_{\mathrm{j}} - 0.3A_{\mathrm{p}}$ to satisfy the condition of $Z_{\mathrm{RE\ loss}} = Z_{\mathrm{NFM18}}$ at $t \sim 7.25$ s. Here, A_{p} is the volume-averaged minor radius of the plasma. Figure 10(e) shows the time evolution of $Z_{\mathrm{RE\ loss}}$. Change in $Z_{\mathrm{RE\ loss}}$ is qualitatively similar to that in the magnitude relation of NFMs shown in Fig. 10(d).

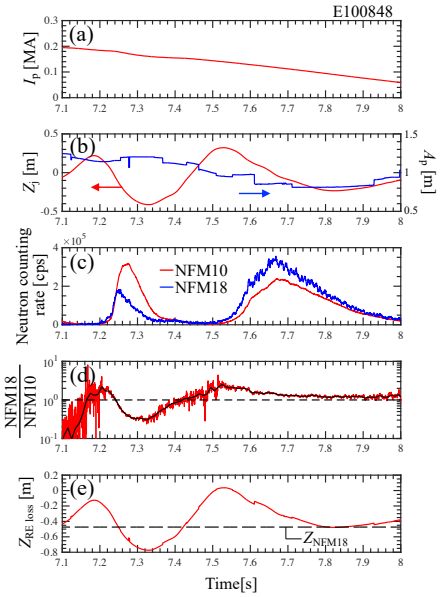

FIG. 10. Time evolution of (a) I_p, (b) Z_j, and the volume-averaged plasma minor radius A_p, (c) neutron counting rates measured with NFM10 (red) and NFM18 (blue), (d) a magnitude relation of neutron counting rates NFM18/NFM10 and (e) the estimated vertical position of the RE loss $Z_{RE\ loss}$ in a typical discharge where the plasma moves vertically due to VDE and REs are lost continuously (E100848). The dashed line in panel (e) represents the vertical position of the NFM18, Z_{NFM18}.

Figure 11 shows the relation between the magnitude relation of NFMs and the estimated $Z_{RE\ loss}$. It is found that there is a positive correlation. The vertical movement of the plasma is detectable using the magnitude relation of NFM signals. In addition, because the almost single correlation is clearly observed, the REs are considered to be lost locally in the poloidal direction on PFC.

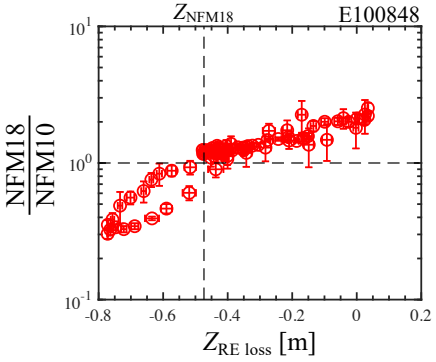

FIG. 11. Relation between magnitude relation of neutron counting rates NFM18/NFM10 and the estimated vertical position of the RE loss $Z_{RE\ loss}$.

5. SUMMARY

Spatiotemporal characteristics of runaway electron (RE) losses observed with neutron flux monitors (NFMs) have been investigated in the integrated commissioning of JT-60SA, i.e., in the first plasma campaign of the large superconducting tokamak, where the available toroidal electric field is limited to be low as well as ITER and DEMO. Even in the low toroidal electric field machine, REs are found to be generated and lost in the case of the low-density plasma, the plasma hitting PFC and the existence of the intense MHD mode. Spatial locality of the RE loss on the PFC can be confirmed based on the magnitude relation of NFM's signals. Installation of dedicated RE diagnostics in JA-DEMO is currently treated as optional, or low priority, in the current design, while NFMs will be installed in JA-DEMO, where available spaces for plasma diagnostics are limited. The results presented here suggests that the NFMs can be effective for RE diagnostics in the non-activation phase of JA-DEMO.

ACKNOWLEDGEMENTS

The author (S. S.) would like to thank Dr. G. Pucella, Dr. A. Matsuyama, Dr. T. Wakatsuki and Dr. S. Nishimura for fruitful discussions. JT-60SA was jointly constructed and is jointly funded and exploited under the Broader Approach Agreement between Japan and EURATOM.

REFERENCES

[1] HENDER, T. *et al*., Nucl. Fusion **47** (2007) S128.
[2] YOSHITA, M. *et al*., Plasma Phys. Control. Fusion **67** (2025) 65010.
[3] WAKATSUKI, T. *et al*., Nucl. Fusion **64** (2024) 104003.
[4] SUKEGAWA, A. M. *et al*., Fusion Eng. Des. **136** (2018) 1653.
[5] NISHITANI, T. *et al*., Rev. Sci. Instrum. **63** (1992) 5270.
[6] ISOBE, M. *et al*., Rev. Sci. Instrum. **85** (2014) 11E114.
[7] YOKOYAMA, T. *et al*., Nucl. Fusion **64** (2024) 126031.
[8] OHTANI, Y. *et al*., Rev. Sci. Instrum. **95** (2024) 073518.
[9] INOUE, S. *et al*., Nucl. Fusion 65 (2025) 036031.
[10] SANO, R. *et al*., Rev. Sci. Instrum. **95** (2024) 073532.
[11] KULSRUD, R. M. *et al.,* Phys. Rev. Lett. **31** (1973) 690.
[12] ROSENBLUTH, M. N. and PUTVINSKI, S. V., Nucl. Fusion **37** (1997) 1355.
[13] TAKECHI, M. *et al*., Fusion Eng. Des. **96-97** (2015) 985.
[14] CAUSA, F. *et al*., Nucl. Fusion **55** (2015) 123021.